



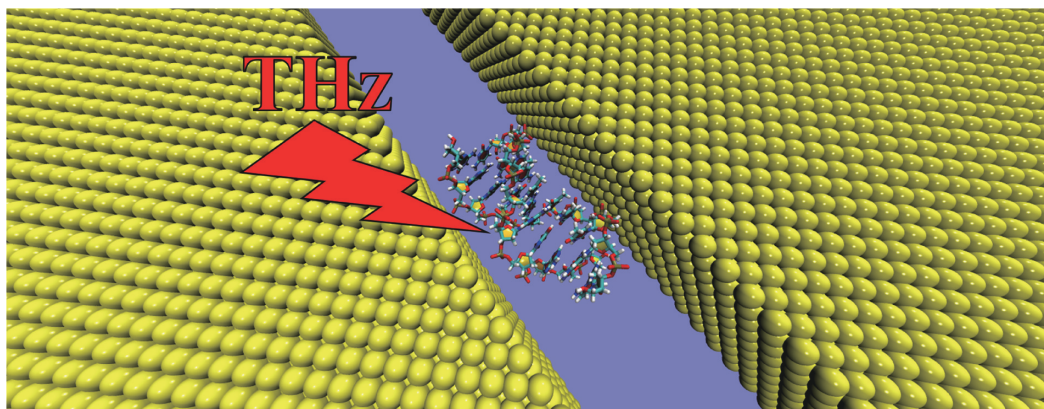
Terahertz Electric Field Induced Double Strand Breakage and Vibrations of dsDNA in a Gold Nanoslit*

JIANG Duan-Jie^{1,2)}, WANG Yan-Hong^{1,2)}, WU Jing-Zhi^{1,2)}**, ZHANG Rui^{1,2)}

⁽¹⁾School of Information and Communication Engineering, North University of China, Taiyuan 030051, China;

⁽²⁾Academy for Advanced Interdisciplinary Research, North University of China, Taiyuan 030051, China)

Graphical abstract



Abstract Objective This work examines the impact of external electric fields at terahertz (THz) frequencies on double-stranded deoxyribonucleic acid (dsDNA) systems adsorbed on Au(111) surfaces in aqueous environments. **Methods** The investigation utilizes a molecular dynamics (MD) approach at the atomic level and vibrational dynamics calculations using the GOLDNA-Amber force field. **Results** The results reveal that the sugar-phosphate backbone of the DNA exhibits reduced adherence to the gold surface, while the side chains display a stronger affinity. When subjecting the hydrated DNA strands to an electric field with frequencies up to 10 THz, peak intensities of vibrational dynamic density (VDoS) are observed at five different frequencies. Moreover, the strong electric field causes hydrogen bonds in the DNA within the slit to break. The sensitivity to the electric field is particularly pronounced at 8.8 THz and 9.6 THz, with different vibrational modes observed at varying electric field strengths. **Conclusion** These findings contribute to an enhanced understanding of the molecular organization of gold-plated charged biological interfaces.

Key words molecular dynamics, electric field, THz spectroscopy, gold surface, low frequency motions

DOI: 10.16476/j.pibb.2024.0064

* This work was supported by a grant from National Defense Science and Technology Innovation Special Zone of China (02-ZT-008).

** Corresponding author.

Tel: 86-13935152056, E-mail: Jingzhi.wu@outlook.com

Received: February 22, 2024 Accepted: April 26, 2024

Deoxyribonucleic acid (DNA) molecules, known as double-helical biopolymers consisting of nucleotides, are renowned for their function as carriers of genetic knowledge^[1-4]. Biological processes such as halogenation, deamination, oxidation, alkylation, and cyanation are intricate alteration mechanisms of DNA, governing crucial life processes such as gene expression, DNA replication, and repair. The accuracy and intricacy of these chemical reactions establish the basis for the genetic variety and adaptability of organisms. Therefore, comprehending the fundamental characteristics of biomolecules is essential for exploring their biological roles.

In recent years, terahertz (THz) spectroscopy has become a robust and efficient approach in complementing traditional detection methods. This technique boasts high sensitivity to subtle changes observed in molecular structures, presenting distinct fingerprint characteristics that effectively depict compound configurations^[5-7]. Both experimental and theoretical investigations have highlighted that the THz spectral attributes are primarily induced by low-frequency intramolecular vibrations stemming from noncovalent interactions, including van der Waals forces, diffusion forces, and hydrogen bonds within the Sub-THz frequency range (0.1–10 THz)^[8]. Chen *et al.*^[9] systematically investigated the molecular mechanisms by which THz waves affect the structure of A β 42 monomer, dimer and tetramer through all-atom molecular dynamics (MD) simulations. It was shown that THz waves at a specific frequency (42.55 THz) could enhance the intramolecular and intermolecular interactions of A β 42 monomer and dimer, respectively, by resonating with the symmetric stretching mode of the —COO— group and the symmetric bending/stretching mode of the —CH₃ group. As a result, the β -structure content in A β 42 monomer is greatly increased and the binding energy between monomers in A β 42 dimer is significantly enhanced. In addition, THz waves mildly stabilize the structure of tetrameric protofibers by enhancing the interactions between peripheral peptides. Wu *et al.*^[10] proposed that THz electromagnetic stimulation also accelerates the process of unspinning the double helix in a physiological environment (room temperature, with the involvement of helicase and ATP), which could contribute to the development of rapid nucleic acid detection devices based on THz technology. In addition, the vibrational modes of these biomolecules

vary in frequency in the THz band and are rich in hydrogen bonds. Combining a specific window of THz-electromagnetic stimulation intensity and frequency is also expected to affect the dynamic behavior of biomolecules, which in turn disrupts their hydrogen bonding and ultimately non-thermal modulation of their structure. Consequently, delving into the THz domain to analyze the peculiarities of biological macromolecules, such as DNA, proves immensely captivating^[11-14].

Nanobiotechnology combined with THz detection, particularly molecular bioelectronics, is a highly promising and rapidly expanding field^[15-18]. Ji *et al.*^[19] proposed a method for THz virus detection that utilizes a nanogap to enhance sensitivity. In this method, the resonance peak of the nanogap exhibits a noticeable red shift when the target virus is present on the nanogap. When the virus is firmly attached to the etched gap, the resonance frequency shift of each virus particle increases by 400%, resulting in further improved sensitivity. Tang *et al.*^[20] combined THz spectroscopy with nanostructures, which not only reduced the strong absorption of water in the THz frequency range but also enabled the specific detection of ssDNA with five base mutations. This was achieved by analyzing the different THz absorption spectra of the four oligonucleotides of ATCG. A nanobiosensor, designed by Keshavarz and Vafapour^[21], consists of an H-shaped graphene resonator on a semiconductor film. This nanobiosensor successfully detects three subtypes of avian influenza (AI) viruses (H1N1, H5N2, and H9N2) in the THz frequency range. The sensitivity of the sensor was as high as 540 GHz/RIU. The development of nanobiotechnology and THz probing has generated great interest. However, the state and nature of biomolecules, such as DNA, in nanostructures are still unclear. MD simulation is a suitable tool for this task, while the nanoslit/DNA work is a good example.

Here, we probe the collective kinetic characteristics of double-stranded DNA molecules in the gold nanoslit at THz frequencies up to 10 THz by employing all-atom MD simulations. To better understand the adsorption relationship between DNA and the gold slit surface under the influence of an electric field, we also calculate the interaction energy between DNA and the gold surface. The simulated structures of DNA are shown in Figure 1.

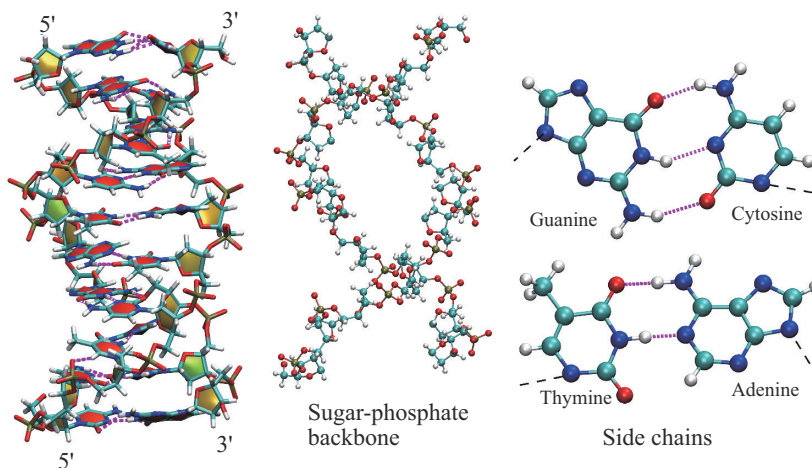


Fig. 1 Studied DNA

Red: oxygen atoms, blue: nitrogen atoms, brown: phosphorus atoms, cyan: carbon atoms, white: hydrogen atoms.

1 Simulation details and methods

The accuracy of interatomic potentials in force fields (FFs) is the key to realistic MD simulations. GoldDNA-Amber FFs account for polarization of the metal atoms and can be parametrized for all the specific interactions found in DNA bases^[22], as GOLP-CHARMM was previously done for peptides^[23-24]. For this work, GoldDNA-Amber is designed for nucleic acids and is compatible with Amber, which is acknowledged as the most reliable classical description of DNA in solution.

Here, we model gold as a five-layer slab with the Au(111) crystal face. Each simulation setup consisted of two Au(111) surfaces, 8.200 nm×5.800 nm, separated by an aqueous solution (Figure 2). At least twice thicker vacuum layer was added to prevent slab-slab interactions through the periodic boundary conditions. The starting configuration of the objective DNA was obtained from the Protein Database Bank (PDB) with entry code 1ZEW (*i. e.*, 10-bp CCTCTAGAGG), which is classified as B-DNA, and topologies were prepared using Sobotop^[25] followed by the manual reassignment of atomic types in accord with GoldDNA-Amber. To conduct the MD simulations, Gromacs 2021.6^[26] was utilized. The molecular representations were visualized using visual molecular dynamics (VMD)^[27].

In order to observe the impact of a THz electric field (THz-EF) stimulus on DNA vibration, we introduced a THz-EF into the entire simulated system. It is worth noting that the dominant force in the interaction between the THz-EF wave and DNA duplexes is the electric component due to the equality of the electric and magnetic components' ratio to the speed of light^[28]. To mimic the THz-EF wave, we utilized the electric field $E(t) = A \cdot u \cdot \cos(\omega t + \varphi)$. A is the amplitude of the electric field, determining the strength of the electric component, while ω denotes the angular frequency, u and φ denote its polarization direction and phase as set to be (1, 0, 0) and 0. The relationship between the angular frequency ω and the EF frequency ν is defined by the equation $\nu = \omega/2\pi$, thus involving the THz-EF stimulus in the molecular dynamics simulation through the electric force associated with E and charges on all atoms. External electric fields with various frequencies were applied to the DNA configuration, with the electric fields predominantly oriented along the x -direction, perpendicular to the gold layer. The frequency range of the applied electric fields fell within 10 THz.

To ensure consistency in simulations, a constant temperature of 298.15 K was maintained utilizing a velocity-rescale thermostat with a coupling time of 0.2 ps. For the treatment of long-range electrostatic interactions, the smooth particle mesh Ewald method was employed^[29-30]. To ensure stability, all bonds

involving hydrogen atoms were constrained using the LINCS algorithm^[31]. The MD time step for all production runs was set to 2 fs. All the FF-based simulations were performed in the canonical ensemble (NVT). After the equilibration, production MD simulation was run for 100 ns.

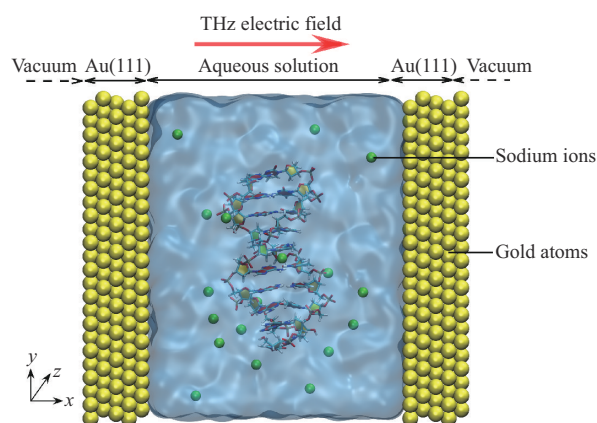


Fig. 2 Representative example of a simulated system demonstrating the computational model: a DNA molecule in aqueous solution between two Au (111) surfaces
Sodium ions and gold atoms are shown as green and yellow spheres.

To study the MD of the simulated system, we define all the dynamic properties calculated for this system, namely the root mean square deviation (RMSD), the root mean square fluctuations (RMSF), the velocity autocorrelation function and the corresponding power spectra.

The RMSD is an important tool that is used to characterize the conformational changes of DNA. It is defined as:

$$RMSD = \sqrt{\frac{1}{N} \sum_{i=1}^N |r_{\text{final}}(i) - r_{\text{initial}}(i)|^2} \quad (1)$$

where N is the number of protein atoms, and $r_{\text{final}}(i)$ and $r_{\text{initial}}(i)$ are the coordinates of an atom i in its final structure and initial structure, respectively. RMSF represent the average changes in atomic positions over time. They provide insight into the flexibility and intensity of movement in both the DNA backbone and side chains during the simulation. It is defined as:

$$RMSF = \sqrt{\frac{1}{T} \sum_{i=1}^T |r_i - r_{\text{initial}}|^2} \quad (2)$$

Where T is the time of simulation. The vibrational

density of states (VDOS) was obtained *via* the Fourier transform of time auto-correlation functions of the atomic velocity V :

$$C_{ps}(\omega) = \int_0^\infty dt \exp(-i\omega t) \langle V(0)V(t) \rangle \quad (3)$$

where $V(t)$ is the atom velocity at time t and the average is taken over different time origins. The velocity autocorrelation functions and the power spectra reveal the microscopic dynamics in liquids.

DNA and the gold surface interacted through the Lennard-Jones (LJ) potential and Coulomb pair potentials. Because these potentials are independent of each other, the total DNA-gold interaction potential energy U is the sum of the LJ U_{LJ} and Coulomb U_{Coul} components. The dependence of U_{LJ} was given by the following:

$$U_{LJ}(r_{ij}) = 4\epsilon_{ij} \left[\left(\frac{\sigma_{ij}}{r_{ij}} \right)^{12} - \left(\frac{\sigma_{ij}}{r_{ij}} \right)^6 \right] = \frac{A_{ij}}{r_{ij}^{12}} - \frac{B_{ij}}{r_{ij}^6} \quad (4)$$

where r_{ij} is the distance between atoms i and j , σ_{ij} is the combined van der Waals radius, and ϵ_{ij} is the depth of the potential well. The distance parameters between different atom types σ_{ij} were obtained through the Lorentz-Berthelot mixing rule, *i. e.*, arithmetic mean. The dependence of U_{Coul} was also modeled with a linear relationship given by the following:

$$U_{Coul}(r_{ij}) = \frac{1}{4\pi\epsilon_0} \frac{q_i q_j}{r_{ij}} \quad (5)$$

$$U_{\text{total}}(r_{ij}) = U_{LJ}(r_{ij}) + U_{Coul}(r_{ij}) \quad (6)$$

where q_i, q_j is the atomic charge and ϵ_0 is the vacuum dielectric constant.

2 Results and discussion

2.1 Simulation result

Adding electric field will alter the distribution of the dipole moment in the DNA molecule, causing its atomic arrangement to align with the direction of the electric field. In Figure 3, the electric field is oriented along the x -axis, which is perpendicular to the gold nano-slit. Simultaneously, the side chains of the bases are attracted to the gold layer, leading to a 90° rotation of the DNA molecule. This rotation gradually stabilizes over time. Before the electric field is applied, the bases at the 3' and 5' ends are absorbed on the gold layer, and the structure is stabilized by hydrogen bonding. After the application of an electric field with THz frequency, the bases at the 3' and 5'

ends are influenced by the electric field, causing the disruption of hydrogen bonding. As a result, they move parallel to the gold layer. Due to the impact of different frequencies on the DNA or backbone and side chains, the electric field force will stretch and straighten the backbone, causing the bases in the

middle section (transparent parts) to rotate and the base pairs at both ends (solid parts) to separate in Figure S1. This implies that the THz electric field at 10 THz affects either the overall or localized vibrational modes.

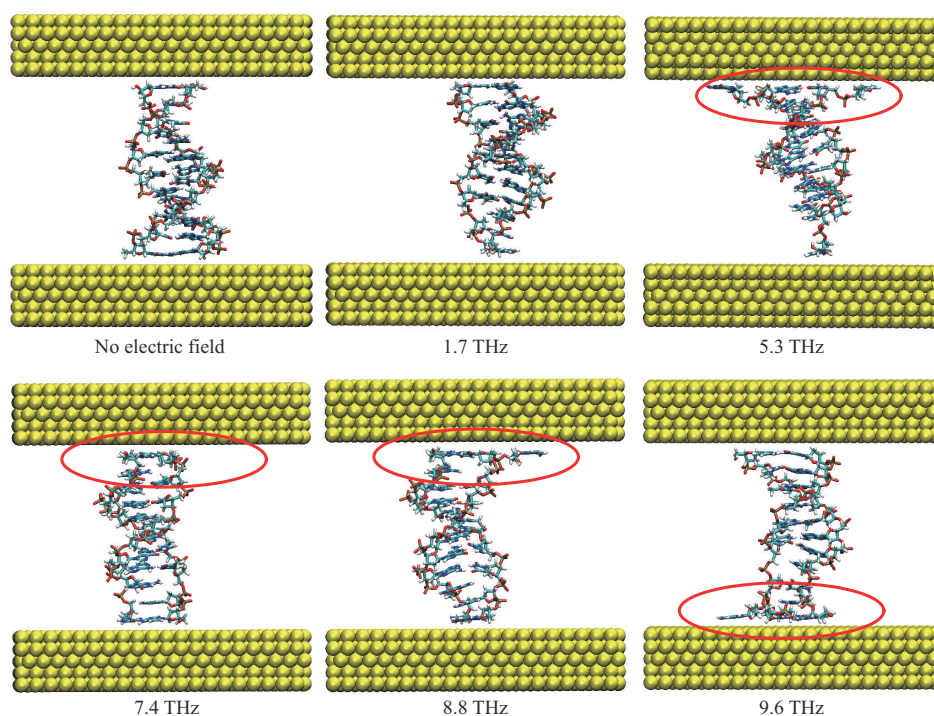


Fig. 3 Final snapshots of DNA molecular conformation (neglecting solvent and equilibrium ions)

Red circles indicate broken hydrogen bonds between base pairs.

2.2 RMSD

The temporal evolution of the RMSD of DNA strands exposed to applied electric fields at various frequencies is depicted in Figure 4. Simulations were obtained from DNA exposed to electric fields with varying frequencies along the x direction. The RMSD of the reference system without electric field, remains stable at approximately 0.3 nm. The fluctuations of the system with THz electric field are larger, but the average value of the RMSD is similar to that of the system without the electric field. This suggests that the stability of entire DNA is not significantly affected by the dramatic fluctuations in its structure after the application of the electric field with amplitude of 0.1 V/nm. It also indicates that the stability of the entire DNA is not greatly compromised by the fluctuations following the application of the electric field. This indicates that the electric field in the THz

frequency range has little impact on the structure of the DNA molecule, despite the significant fluctuations in its structure. The root mean square deviation increases from 0.3 nm to 0.4 nm at 1.7 THz and 5.3 THz, respectively. This suggests that the THz electric field affects the backbone or side strands, causing the overall DNA structure to change, and a comparison with the final snapshot shows that the ends of the DNA are the most affected.

To delve deeper into the impact of an electric field on DNA structure, we analyze the changes in the RMSD of the sugar-phosphate backbone and base side chains at varying frequencies of the electric field, as illustrated in Figure 4. The RMSD values of the backbone and side chains reduce to 0.1 nm post adsorption onto the gold nanolayer (Figure 4a). Both components exhibit simultaneous changes without altering the overall DNA structure. An increase in

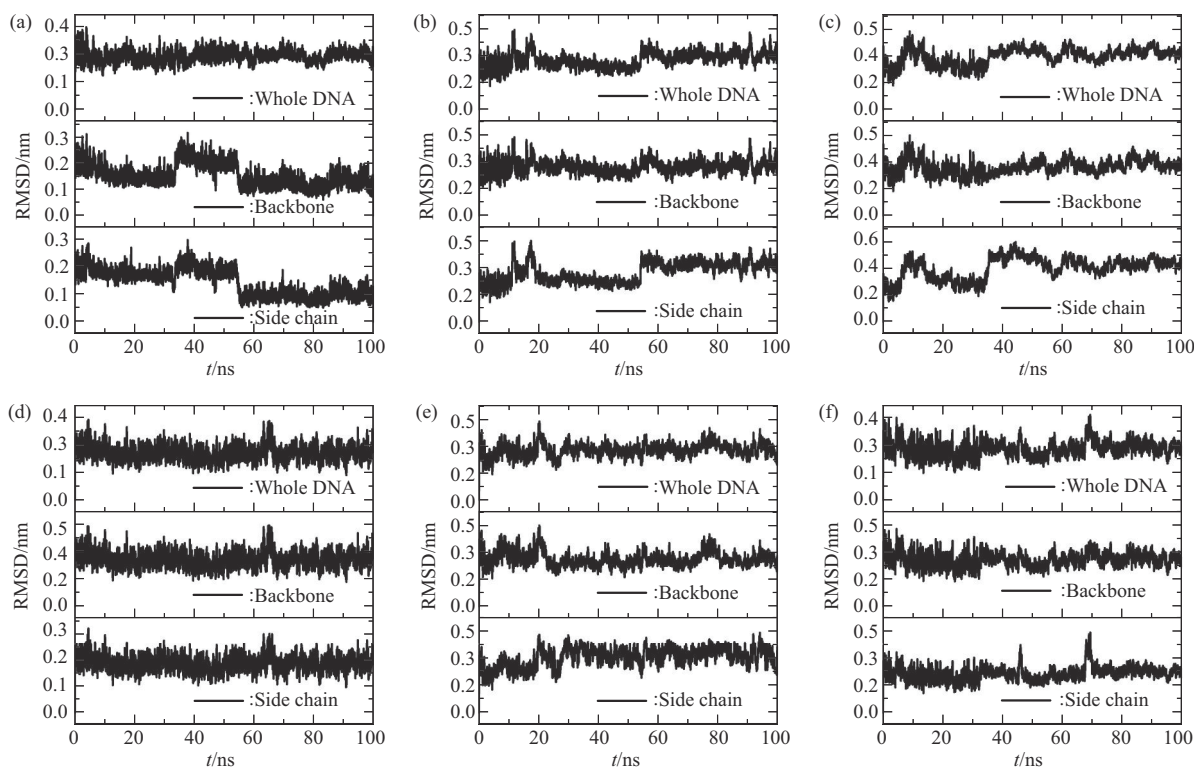


Fig. 4 RMSD at different electric field frequencies

(a) No electric field applied, (b) 1.7 THz, (c) 5.3 THz, (d) 7.4 THz, (e) 8.8 THz, (f) 9.6 THz.

RMSD of the side chains during the 50–60 ns timeframe affects the entire DNA molecule. This indicates that electric fields at 1.7 THz (Figure 4b), 5.3 THz (Figure 4c), and 9.6 THz (Figure 4f) predominantly impact the side chains of DNA bases, making a substantial contribution. A sudden rise in RMSD of the backbone and side chains is observed between 60–70 ns, influencing the overall DNA structure (Figure 4d). Figure 4e demonstrates a notable peak in the RMSD value of the backbone between 70–80 ns due to the electric field at 8.8 THz, also affecting the DNA structure.

We demonstrate the impact of various directions and intensities of electric fields on DNA (Figure S2). In the first 10 ns, the RMSD of Figure S2a,b exhibits a significant variation ranging from 0.2–0.4 nm. This indicates the presence of intense movement of the DNA strands within the gold nanoslit. In the meantime, the DNA gradually adsorbed onto the gold layer, which is a process of progressively enhancing the interaction between DNA and gold. Although we made changes in the direction and intensity, the “firmness” between the DNA and the slit is difficult

to break, and the final value of the RMSD stabilizes at about 0.3 nm.

2.3 RMSF

RMSF provides information about the dynamics of different regions or atoms within a biomolecule. Regions with high RMSF indicate that these areas experienced significant fluctuations during the simulation. These fluctuations may be linked to structural changes or specific biological processes. In Figure 5, the bases at the 3' and 5' ends of the DNA fluctuate more because the side chains of the DNA bases at the ends are absorbed on the gold nanolayer. These bases (atom index 283–316, guanine; atom index 317–344, cytosine; atom index 1–28, cytosine; atom index 599–632, guanine) are free from hydrogen bonding between the bases, making them more “flexible” compared to the bases in the middle portion. The THz electric field has a great effect on the two ends of the DNA molecule, *i.e.*, the 3' end and the 5' end, and the RMSF values of both regions are higher than the other positions (Figure 5), but it is found from the simulation process that the THz electric field affects the two ends of the DNA in two

conditions, one is a single end, and the other is that the two ends are subjected to the electric field effect at the same time. This is consistent with the structural changes of the DNA in the final snapshot, where the fluctuation of the C-G of the bases at both ends of the

DNA at an electric field frequency of 1.7 THz is significantly smaller than at other frequencies. This suggests that the low frequency is not sufficient to break the hydrogen bonds between the bases at the same electric field strength.

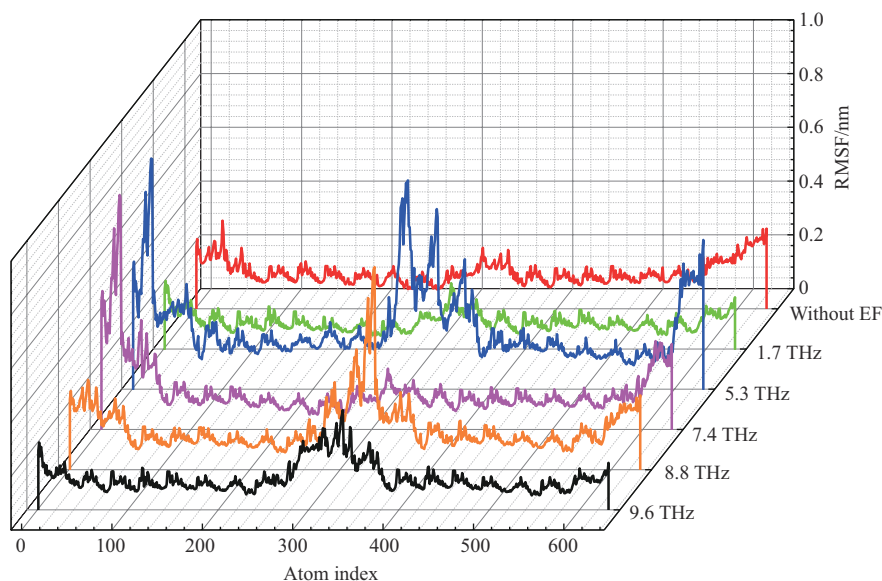


Fig. 5 RMSF at different electric field frequencies

2.4 Vibrational density of states (VDoS)

We calculated the VDoS for DNA in 4 nm gold slit (Figure 6), where the VDoS spectra of the sugar-phosphate backbone exhibit peak intensities at frequencies around 1.7, 5.3 and 7.4 THz. Meanwhile, the VDoS spectra of the side chains show peak intensities at frequencies around 1.7, 5.3, 7.4, 8.8 and 9.6 THz. Consequently, the VDoS spectra of the entire DNA strand display five peaks at frequencies of 1.7, 5.3, 7.4, 8.8 and 9.6 THz, respectively. This is the same conclusion as in previous studies^[32]. Within 1–3 THz, there is a broad overlapping peak attributed mainly to the DNA backbone and side chains. The peak intensity at 9.6 THz in the side chain is not clearly distinguishable. Examination of the complete power spectrum indicates that as THz frequency increases, DNA transitions from collective vibration to local vibration. In the low-frequency range (below 5 THz), the collective vibration of DNA is easily affected by the surrounding environment (water and the gold slit), resulting in restricted movement and a decrease in the number of modes in this range.

The VDoS of the sugar-phosphate backbone is

shown to be influenced downward by the electric field, in contrast to the base side chains (Figure 6). Peaks in the DNA power spectra arise from contributions of both the backbone and side chains. When subjected to the electric field at the peak frequency, these two components exhibit distinct responses, largely due to differences in vibrational frequencies. Following the introduction of THz electric fields, notable peak shifts were observed in the DNA strands and side chains at corresponding frequencies, while the VDoS spectra of the backbone remained relatively unaffected. These findings suggest that THz electric fields primarily impact the base side chains, leaving the backbone relatively stable. The VDoS peaks at all five corresponding frequencies are significantly increased by tens or even hundreds of times when an electric field is applied, indicating an enhancement in the collective vibration of DNA. Comparing Figure 6b–f, it is evident that the VDoS of the DNA backbone and side strand are relatively low, especially for the DNA and side strand. Analysis of the final snapshots and RMSF suggests that the increased VDoS peak is a result of hydrogen

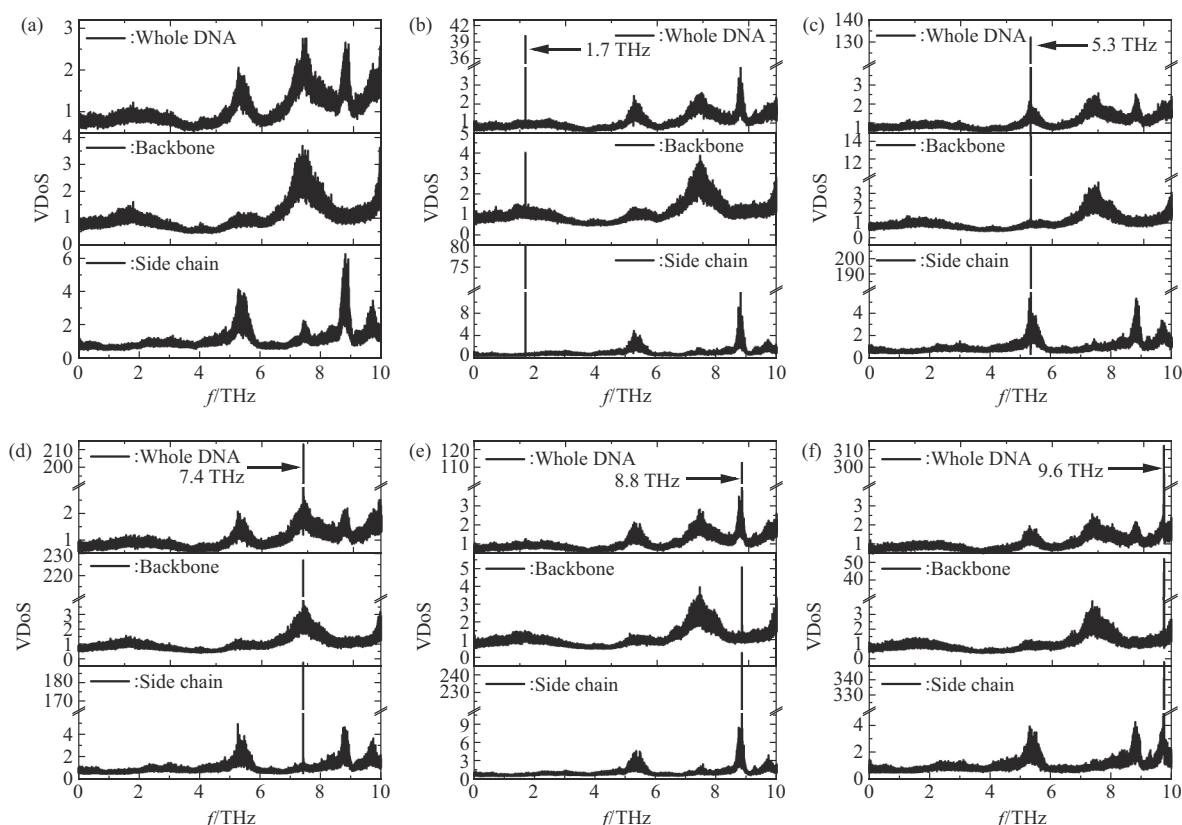


Fig. 6 VDoS at different electric field frequencies at 0.1 V/nm

(a) No electric field applied, (b) 1.7 THz, (c) 5.3 THz, (d) 7.4 THz, (e) 8.8 THz, (f) 9.6 THz.

bond breaking between the base pairs at both ends of the DNA, except at a frequency of 1.7 THz. Further examination under different electric field strengths depicted in Figure S3 reveals that the peaks at each frequency notably increase when the electric field strength is 0.5 V/nm. This implies that at this level of electric field strength in the gold slit, hydrogen bonds between DNA strands break at any frequency. As the electric field strength decreases, the VDoS also decreases, although hydrogen bond breaking still occurs. For instance, at an electric field strength of 0.05 V/nm, hydrogen bond breaking ceases at the electric field frequencies of 1.7, 5.3, and 7.4 THz. This continues until the electric field strength decreases to 0.01 V/nm, at which point it completely disappears. The variation of the VDoS at different frequencies under varying electric fields is illustrated in Figure 7a. As the strength of the electric field decreases, the VDoS at different frequencies also decreases significantly. Notably, there is a tenfold difference in electric field strength between 0.5 V/nm and 0.05 V/nm, resulting in a thousandfold change in amplitude. Similarly, there is a hundredfold amplitude

change between 0.1 V/nm and 0.01 V/nm. Meanwhile, the VDoS values at all five frequencies show an upward trend. The frequency of the electric field jumps to 5.3 THz when the electric field strength is 0.1 V/nm, and it jumps to 8.8 THz when the electric field strength is 0.05 V/nm. From the spectra shown in Figure 7a and VDoS, when the frequencies are 8.8 THz and 9.6 THz, the VDoS at these two frequencies increases with the electric field strength and the multiplicity of the increase is tens of times that of other frequencies. And the slopes of the curves with increasing electric field strength are larger than the other frequencies for both 8.8 THz and 9.6 THz (Figure 7a). It can be observed that frequencies of 8.8 THz and 9.6 THz are more sensitive to the electric field than other frequencies. Figure 7b–e and Figure S4 demonstrate the vibrational direction of the hydrogen-bond breaking portion of the DNA at frequencies of 8.8 THz and 9.6 THz, respectively. The free bases on the gold layer, which are the part of the hydrogen bond that is broken, vibrate in a rotational twist around the DNA spindle. This information is helpful for us in our search for a THz electric field

that is suitable for detecting the collective vibration of DNA. The snapshots of hydrogen bond breakage are

shown in detail in Figure S5.

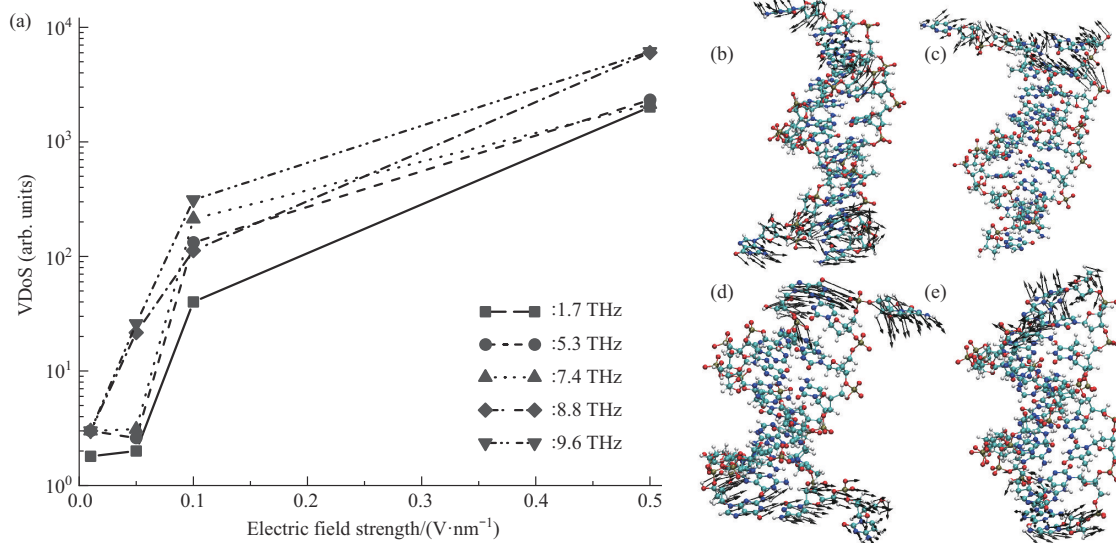


Fig. 7 Relationship between VDoS values and electric field strength and frequency

(a) VDoS at different frequencies and electric field strengths, (b–e) vibrational direction of the broken portion of the hydrogen bond at 8.8 THz, 0.5 V/nm (b), 0.1 V/nm (c), 0.05 V/nm (d), 0.01 V/nm (e).

We investigated the effects of the gold slit width and electric field strength on the collective vibrational modes of DNA (Figure 8). The VDoS of DNA decreases with increasing slit width and increases with increasing electric field strength over the entire frequency range. As the width of the gold slit increases, the thickness of the water layer where the DNA is located also increases (Figure 8a). Sufficient water leads to a decrease in the value of the VDoS, and the peak intensity generated by the excitation of the DNA molecules is significantly reduced after the addition of an electric field with a frequency of 1.7 THz. This suggests that, in addition to the restriction of the DNA collective vibration caused by the removal of the gold layer, the DNA molecules are also confined within the water network. After adding an electric field of 1.7 THz and varying the intensity, the peak intensity produced at 1.7 THz increases with the increase in electric field intensity (Figure 8b). Additionally, the collective vibration of DNA at 1.7 THz is also enhanced. It should be noted that the width of the gold nanoslit and the electric field strength did not have an effect on the frequency shift of the VDoS. All the peaks remained in the same position, indicating that changes in the width of gold slit and strength of electric field did not significantly

alter the vibrational dynamics of the DNA.

2.5 Interaction energy

The presence of an external electric field has a profound effect on intermolecular interactions, particularly by inducing electric dipole moments in molecules and causing electric field-induced interactions, which influences the movement of electrons within the molecule. When an external electric field is applied to a molecule, it directly affects the distribution of the electron cloud within the molecule. This causes the positive and negative charge centers in the molecule to shift in the direction of the electric field. This electric field-induced electric dipole moment plays a crucial role in molecular interaction process. Such changes in the electric dipole moment can trigger attractive or repulsive forces between molecules, which can affect their orientation and alignment^[33-34]. In Figure 9, the more negative the value, the stronger the interaction between DNA and the gold layer. The electric field at THz frequency mainly affects the collective vibration of DNA and does not significantly alter the overall electronic distribution of DNA. The change in the total dipole moment is minimal, resulting in the total energy remaining near -800 kJ/mol. This can be observed from the final snapshots in Figure 3.

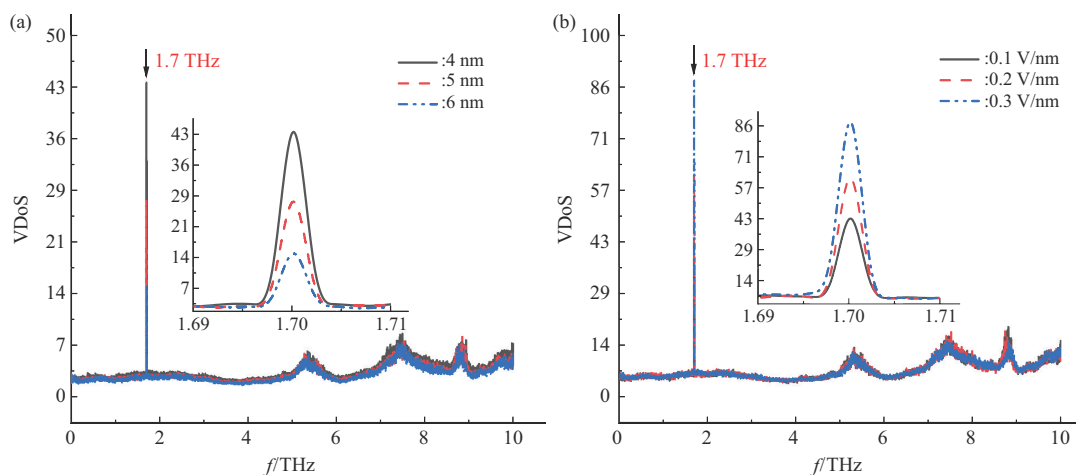


Fig. 8 VDoS at different slit widths or electric field strengths

(a) Width of slit, (b) strength of electric field.

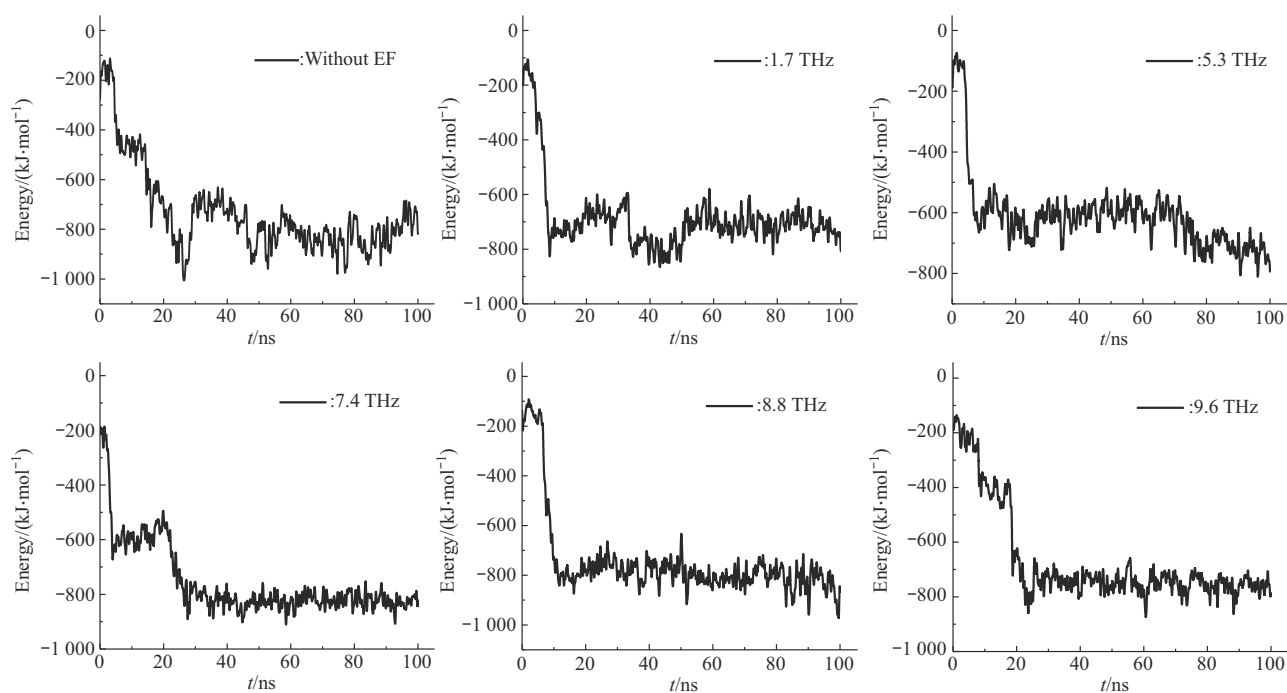


Fig. 9 Total interaction energy at 0.1 V/nm

3 Conclusion

This study investigates the collective vibrational modes of DNA in nanogold using molecular dynamics simulations under THz electric fields. The analysis reveals that the backbone and side chains of DNA contribute differently to the vibrational dynamics. As the electric field strength increases, the contribution to

the collective vibration of DNA also increases; however, it is important to note that a strong electric field may result in the breaking of hydrogen bonds within DNA. This effect diminishes as the electric field strength decreases. Moreover, the study identifies rotationally twisted vibration modes at frequencies of 8.8 THz and 9.6 THz under different electric fields. Additionally, the interaction between

DNA and the gold layer is quantitatively evaluated, providing valuable insights into the structural changes of DNA molecules in nanostructures. Gold layers play a key role in THz biosensors as a source and enhancement medium of electric fields. Understanding the interaction mechanism between DNA molecules and the gold layer is of crucial importance for designing THz biosensors with high sensitivity and specificity.

Supplementary Available online (<http://www.pibb.ac.cn>, <http://www.cnki.net>):

PIBB_20240064_Figure_S1.pdf

PIBB_20240064_Figure_S2.pdf

PIBB_20240064_Figure_S3.pdf

PIBB_20240064_Figure_S4.pdf

PIBB_20240064_Figure_S5.pdf

参 考 文 献

- [1] Nowak E, Wisła-Świder A, Khachatryan G, *et al.* Possible sensor applications of selected DNA-surfactant complexes. *Eur Biophys J*, 2019, **48**(4): 371-381
- [2] Yan H. Nucleic acid nanotechnology. *Science*, 2004, **306**(5704): 2048-2049
- [3] Pandey P K, Rawat K, Aswal V K, *et al.* Imidazolium based ionic liquid induced DNA gelation at remarkably low concentration. *Colloids Surf A Physicochem Eng Aspects*, 2018, **538**: 184-191
- [4] Chworos A, Severcan I, Koyfman A Y, *et al.* Building programmable jigsaw puzzles with RNA. *Science*, 2004, **306**(5704): 2068-2072
- [5] Markelz A, Whitmire S, Hillebrecht J, *et al.* THz time domain spectroscopy of biomolecular conformational modes. *Phys Med Biol*, 2002, **47**(21): 3797-3805
- [6] Wang F, Zhao D, Dong H, *et al.* Terahertz spectra of DNA nucleobase crystals: a joint experimental and computational study. *Spectrochim Acta A Mol Biomol Spectrosc*, 2017, **179**: 255-260
- [7] Woods K N. THz time scale structural rearrangements and binding modes in lysozyme-ligand interactions. *J Biol Phys*, 2014, **40**(2): 121-137
- [8] Wang F, Jiang L, Song J, *et al.* Sub-THz spectroscopic characterization identification for pine wood nematode ribosomal DNA. *Spectrochim Acta A Mol Biomol Spectrosc*, 2020, **232**: 118152
- [9] Chen C, Yan Z S, Ma Y Q, *et al.* Effect of terahertz waves on the structure of the A β 42 monomer, dimer, and protofibril: insights from molecular dynamics simulations. *ACS Chem Neurosci*, 2023, **14**(23): 4128-4138
- [10] Wu K, Qi C, Zhu Z, *et al.* Terahertz wave accelerates DNA unwinding: a molecular dynamics simulation study. *J Phys Chem Lett*, 2020, **11**(17): 7002-7008
- [11] Tang M, Huang Q, Wei D, *et al.* Terahertz spectroscopy of oligonucleotides in aqueous solutions. *J Biomed Opt*, 2015, **20**(9): 095009
- [12] Fischer B M, Walther M, Uhd Jepsen P. Far-infrared vibrational modes of DNA components studied by terahertz time-domain spectroscopy. *Phys Med Biol*, 2002, **47**(21): 3807-3814
- [13] Pickwell-MacPherson E, Wallace V P. Terahertz pulsed imaging—a potential medical imaging modality?. *Photodiagnosis Photodyn Ther*, 2009, **6**(2): 128-134
- [14] Zhang C, Yuan Y, Wu K, *et al.* Driving DNA origami assembly with a terahertz wave. *Nano Lett*, 2022, **22**(1): 468-475
- [15] Seo M, Park H R. Terahertz biochemical molecule-specific sensors. *Adv Opt Mater*, 2020, **8**(3): 1900662
- [16] Liu X, Qiao Z, Chai Y, *et al.* Nonthermal and reversible control of neuronal signaling and behavior by midinfrared stimulation. *Proc Natl Acad Sci USA*, 2021, **118**(10): e2015685118
- [17] Lou J, Jiao Y, Yang R, *et al.* Calibration-free, high-precision, and robust terahertz ultrafast metasurfaces for monitoring gastric cancers. *Proc Natl Acad Sci USA*, 2022, **119**(43): e2209218119
- [18] Jiao Y, Lou J, Ma Z, *et al.* Photoactive terahertz metasurfaces for ultrafast switchable sensing of colorectal cells. *Mater Horiz*, 2022, **9**(12): 2984-2992
- [19] Ji G, Kim H S, Cha S H, *et al.* Terahertz virus-sized gold nanogap sensor. *Nanophotonics*, 2023, **12**(1): 147-154
- [20] Tang M, Zhang M, Yan S, *et al.* Detection of DNA oligonucleotides with base mutations by terahertz spectroscopy and microstructures. *PLoS One*, 2018, **13**(1): e0191515
- [21] Keshavarz A, Vafapour Z. Sensing avian influenza viruses using terahertz metamaterial reflector. *IEEE Sens J*, 2019, **19**(13): 5161-5166
- [22] Rosa M, Corni S, Di Felice R. Enthalpy-entropy tuning in the adsorption of nucleobases at the Au(111) surface. *J Chem Theory Comput*, 2014, **10**(4): 1707-1716
- [23] Wright L B, Rodger P M, Corni S, *et al.* GoIP-CHARMM: first-principles based force fields for the interaction of proteins with Au(111) and Au(100). *J Chem Theory Comput*, 2013, **9**(3): 1616-1630
- [24] Wright L B, Rodger P M, Walsh T R, *et al.* First-principles based force fields for the interaction of proteins with Au(100) (5 \times 1): an extension of GoIP-CHARMM. *J Phys Chem C*, 2013, **117**(46): 24292-24306
- [25] Tian Lu, Sobtop, Version 1.0, <http://sobereva.com/soft/Sobtop> (accessed on November 16, 2023)
- [26] Abraham M J, Murtola T, Schulz R, *et al.* GROMACS: high performance molecular simulations through multi-level parallelism from laptops to supercomputers. *SoftwareX*, 2015, **1**: 19-25
- [27] Humphrey W, Dalke A, Schulten K. VMD: visual molecular dynamics. *J Mol Graph*, 1996, **14**(1): 33-38, 27-28
- [28] Zhu Z, Chang C, Shu Y, *et al.* Transition to a superpermeation phase of confined water induced by a terahertz electromagnetic

- wave. *J Phys Chem Lett*, 2020, **11**(1): 256-262
- [29] Essmann U, Perera L, Berkowitz M L, *et al.* A smooth particle mesh Ewald method. *J Chem Phys*, 1995, **103**(19): 8577-8593
- [30] Yeh I C, Berkowitz M L. Ewald summation for systems with slab geometry. *J Chem Phys*, 1999, **111**(7): 3155-3162
- [31] Hess B, Bekker H, Berendsen H J C, *et al.* LINCS: a linear constraint solver for molecular simulations. *J Comput Chem*, 1997, **18**(12): 1463-1472
- [32] Singh A K, Wen C, Cheng S, *et al.* Long-range DNA-water interactions. *Biophys J*, 2021, **120**(22): 4966-4979
- [33] Bekard I, Dunstan D E. Electric field induced changes in protein conformation. *Soft Matter*, 2014, **10**(3): 431-437
- [34] Hardt S, Hartmann J, Zhao S, *et al.* Electric-field-induced pattern formation in layers of DNA molecules at the interface between two immiscible liquids. *Phys Rev Lett*, 2020, **124**(6): 064501

太赫兹电场诱导金纳米狭缝中双链DNA的 氢键断裂和振动*

姜端杰^{1,2)} 王艳红^{1,2)} 武京治^{1,2)**} 张 瑞^{1,2)}

⁽¹⁾ 中北大学信息与通信工程学院, 太原 030051;

⁽²⁾ 中北大学前沿交叉科学技术研究院, 太原 030051)

摘要 **目的** 本文探讨了太赫兹 (THz) 频率下的外电场对吸附在金(111)表面的水合双链脱氧核糖核酸 (dsDNA) 系统的影响。**方法** 采用GoIDNA-Amber力场进行分子动力学模拟。**结果** DNA的碱基侧链比糖磷酸骨架更容易吸附在金层表面。当水合DNA分子置于频率高达10 THz的电场中时, 振动态密度 (VDoS) 分别在5个不同频率下观察到峰值强度。此外, 强电场会导致狭缝内DNA双链之间的氢键断裂。此现象在8.8 THz和9.6 THz的电场频率下尤为明显, 并且在不同的电场强度下展示出不同的振动模式。**结论** 这些发现有助于加深对镀金生物界面的分子组织的理解。

关键词 分子动力学, 电场, 太赫兹光谱, 金层, 低频运动

中图分类号 Q617, Q615

DOI: 10.16476/j.pibb.2024.0064

* 国防科技创新特区 (02-ZT-008) 资助项目。

** 通讯联系人。

Tel: 13935152056, E-mail: Jingzhi.wu@outlook.com

收稿日期: 2024-02-22, 接受日期: 2024-04-26